Clim. Past Discuss., 10, 1653–1673, 2014
www.clim-past-discuss.net/10/1653/2014/
doi:10.5194/cpd-10-1653-2014

Climate of the Past
Discussions
Open Access

The impact of Sahara desertification on Arctic cooling during the Holocene

F. J. Davies[1], **H. Renssen**[1], **M. Blaschek**[1], **and F. Muschitiello**[2,3]

[1]Department of Earth Sciences, Faculty of Earth and Life Sciences, Vrije Universiteit Amsterdam, 1081HV Amsterdam, the Netherlands
[2]Bolin Centre for Climate Research, Stockholm University, 106 91 Stockholm, Sweden
[3]Department of Geological Sciences, Stockholm University, 106 91 Stockholm, Sweden

Received: 15 March 2014 – Accepted: 29 March 2014 – Published: 11 April 2014

Correspondence to: F. J. Davies (f.j.davies@vu.nl)

Published by Copernicus Publications on behalf of the European Geosciences Union.

The impact of Sahara desertification on Arctic cooling during the Holocene

F. J. Davies et al.

Abstract

Since the start of the Holocene, temperatures in the Arctic have steadily declined. This has been accredited to the orbitally forced decrease in summer insolation reconstructed over the same period. However, we present climate modelling results here that indicate that up to 42 % of the cooling in the Arctic, over the period 9–0 ka was a direct result of the desertification that occurred in the Sahara. Through a land–atmosphere teleconnection, increasing surface albedo in the Sahara leads to a regional increase in surface pressure, a weakening of the trade winds, the westerlies and the polar easterlies, which in turn reduces the meridional heat transported by the atmosphere to the Arctic. Additionally, through a series of targeted sensitivity experiments we explored the affects that using a modern cloud data set has upon mid and early Holocene climate simulations, and show that despite an apparent weakness in our model our original conclusions are robust. We conclude that interglacial climate is sensitive to changes in Sahara vegetation type, which has significance in the future debate of the response of the Sahara to climate change, considering the uncertainty surrounding future precipitation projections for this region.

1 Introduction

The Holocene is characterized by an early thermal maximum (~ 11–6 ka) in the Northern Hemisphere, followed by gradually declining global temperatures that persisted up until the recent period of anthropogenically induced warming. This cooling was most prevalent in the high northern latitudes with July temperatures, north of 60° N, decreasing by 3–4 °C from 9 to 0 ka (Renssen et al., 2005) and has been attributed to the orbitally forced reduction in summer insolation (Renssen et al., 2005, 2009), decreasing by 42 $W m^{-2}$ over this period at 65° N (Berger, 1978). The early Holocene positive summer insolation anomaly also had a strong impact on the vegetation in Northern Africa through a strengthening of the summer monsoons, leading to

CPD
10, 1653–1673, 2014

enhanced precipitation and grassland vegetation in the Sahara region (Kutzbach and Street-Perrott, 1985). This phase is often referred to as the African Humid Period (AHP), which lasted until the mid-Holocene, although the exact timing of its demise and the subsequent rate at which it occurred is still a contentious issue (deMenocal et al., 2000; Kröpelin et al., 2008). Following the AHP, the Sahara, under the influence of the long-term decline in summer insolation, evolved into a desert environment.

Previous studies have shown that drastic vegetation changes in the Amazon can influence winter precipitation in the North Atlantic and Europe, which are brought about due to large-scale circulation changes in the mid and high latitudes (Gedney and Valdes, 2000). Therefore, with the Sahara being the world's largest non-polar desert, it is entirely plausible that changes in its surface albedo, caused by the large-scale shift in vegetation during the Holocene, could have profound effects on global climate. Accordingly, in this study, we have performed climate model experiments to analyse how Sahara vegetation changes during the Holocene have contributed to cooling in the Arctic (defined herein as north of 66.5° N).

2 Model and experimental design

2.1 Model

We applied LOVECLIM, an earth model of intermediate complexity (Goosse et al., 2010), which is comprised of a coupled atmosphere, ocean, sea-ice and vegetation model. The atmospheric component, ECBilt, is a quasi-geostrophic dynamical atmosphere with a horizontal T21 truncation and three vertical layers, 800, 500, and 200 hPa (Haarsma et al., 1996; Opsteegh et al., 1998) and includes a full hydrological cycle. Clouds are prescribed based on the ISCCP D2 dataset (1983–1995) from Rossow (1996), with the total upward and downward radiative fluxes computed as a function of this dataset. The oceanic component, CLIO, is a primitive-equation, free-surface general ocean circulation model (Deleersnijder and Campin,

CPD
10, 1653–1673, 2014

1995; Deleersnijder et al., 1997) coupled to a thermodynamic-dynamic sea-ice model (Fichefet and Morales Maqueda, 1997, 1999), and has a resolution of 3° × 3° latitude-longitude and realistic bathymetry. The vegetation component, VECODE, is a reduced form dynamic global vegetation model, and is capable of simulating the dynamics of two plant functional types, trees and grasses, as well as desert as a dummy type (Brovkin et al., 2002). These vegetation types have an effect on the surface albedo, soil moisture content, and net precipitation.

2.2 Experimental design

In order to calculate the contribution of Sahara desertification on cooling in the Arctic during the Holocene, a series of experiments were designed. An initial transient simulation (OG) from 9 to 0 ka was performed, forced with appropriate orbital parameter settings (Berger, 1978) and greenhouse gas concentrations (Loulergue et al., 2008; Schilt et al., 2010), whilst the solar and volcanic forcings were fixed at preindustrial conditions. In addition, another simulation (OGGIS), which included the same forcings as OG, plus additional Laurentide (LIS) and Greenland (GIS) Ice Sheet meltwater fluxes and topography changes, was performed. The LIS meltwater fluxes were based on the reconstructions of Licciardi et al. (1999) and those for the GIS on Blaschek and Renssen (2013). The associated topographic and surface albedo changes of the LIS were based on reconstructions by Peltier (2004) and applied at 50 year time steps. However, GIS topographic changes were not accounted for because the changes are only minor at the spatial resolution of our model. For a more detailed description of the experimental setup of OGGIS the reader is referred to Blaschek and Renssen (2013). In both OG and OGGIS, global 9 to 0 ka vegetation changes were calculated interactively using VECODE.

These simulations allowed us to simulate the natural vegetation evolution over the Holocene in the Sahara region. From these simulations we were able to evaluate the relative vegetation fractions that were present in both the OG and OGGIS simulations at 9, 6, and 0 ka. Following this, a series of equilibrium experiments were performed with fixed Saharan vegetation (Table 1). The relative percentages of Saharan vegetation cover at 9, 6 and 0 ka taken from both OG and OGGIS were combined with orbital and trace gas levels for 9, 6, and 0 ka, which followed the guidelines of PMIP3 (http://pmip3.lsce.ipsl.fr/), resulting in a total of 18 equilibrium experiments. All equilibrium simulations were ran from a control pre-industrial simulation for 2500 years, allowing the model, in particular the deep oceans, to reach a quasi-equilibrium state (c.f. Renssen et al., 2006). For the OGGIS equilibrium simulations LIS and GIS topography were kept constant, however LIS and GIS melt fluxes were not included. Including them would result in the constant addition and freshening of the ocean, which in turn would prevent the oceans, in particular the deep oceans, in reaching a quasi-equilibrium state, therefore, rendering those particular equilibrium experiments unrealistic. Neglecting the melt fluxes likely resulted in a marginally warm early Holocene climate in our 9k9kEQ_OGGIS equilibrium experiments.

From the OG and OGGIS equilibrium experiments we were able to deduce the contribution of Sahara desertification to Arctic cooling during the Holocene (Appendix A). Data presented are averages over the last 500 years of each simulation. To investigate an “extreme” example of Sahara desertification between the mid and late Holocene, we also performed 6 equilibrium simulations that had 100 % grass and desert in the Sahara at 9, 6, and 0 ka, (Table 2). In LOVECLIM the albedo of grass and desert are 0.2 and 0.4 respectively. The Sahara was defined as 15° W–35° E and 11–33° N.

3 Results and discussion

Our results for both the OG and OGGIS equilibrium experiments can be separated into two distinct phases, 9–6 ka and 6–0 ka (Fig. 1a and b). In the OG experiment there is a total 9–0 ka cooling in the Arctic of 2.9 °C (Figs. 1a and 2a), with 0.7 °C occurring between 9 and 6 ka and 2.1 °C between 6 and 0 ka. Of this total cooling, 2.1 °C is due

CPD
10, 1653–1673, 2014

The impact of Sahara desertification on Arctic cooling during the Holocene

F. J. Davies et al.

to direct orbital and greenhouse gas forcing (Figs. 1b and 2b), whilst 0.5 °C (17 %) is due to Sahara desertification alone (Figs. 1a and 2c).

In the OGGIS transient experiment, the 9 ka climate is relatively cold due to the cooling effect of the LIS and GIS, leading to a delayed thermal maximum over most of the Arctic (Renssen et al., 2009). Because of the cooler early Holocene climate, we find a total warming of 1.0 °C from 9 to 6 ka (Fig. 1b). However, the difference in Sahara vegetation had a cooling effect of 0.2 °C between 9 and 6 ka and without this moderating effect, the warming would have even been higher (1.3 °C).

The second phase, 6 to 0 ka, of the OGGIS equilibrium experiment was identical to the OG equilibrium experiment, with a total decrease in mean annual Arctic temperature of 2.1 °C, with 0.4 °C due to desertification in the Sahara and the remainder of the cooling due to the localised effects of insolation changes. Therefore it can be said that for the OG experiment from 9 to 0 ka, 17 % of the observed cooling was a direct consequence of desertification in the Sahara. In the OGGIS experiment Sahara desertification suppressed the warming by 15 % between 9 to 6 ka, and from 6 to 0 ka was responsible for 19 % of the observed cooling in the Arctic.

The cooling in the Arctic is a consequence of Sahara desertification, which invokes a land–atmosphere teleconnection. Due to the prescribed desertification in the Sahara in our equilibrium simulations, over the course of the Holocene net albedo and radiative heat loss increases, leading to a decrease in surface temperatures and an increase in surface pressure in the Sahara. The decreasing temperatures in the Sahara cause an increase in the surface pressure (Fig. 3) with an extension over the Tropical Atlantic, leading to an easterly zonal shift, plus an expansion, of the Azores high. Additionally, we observe a weakening of the low latitude trade winds and a net overall decrease in the atmospheric meridional heat flux (Fig. 4). In particular we observe a weakening of the mid-latitude westerlies. This overall weakening of the winds and atmospheric heat transport over the Atlantic Ocean is consistent with a decrease in the meridional temperature gradient due the relatively strong cooling over the Sahara. As a result, the Icelandic Low stabilises, which in turns results in a weakening of

CPD
10, 1653–1673, 2014

the polar easterlies. The Bjerknes compensation theory suggests that a weakened atmospheric heat transport would be compensated by an increase in oceanic heat transport (Bjerknes, 1964). This is indeed what we observe (Fig. 4), however the increase in oceanic heat transport (0.058 PW at 7° N, before gradually reducing to 0 PW in the Arctic) is less than the atmospheric decreases, resulting in an overall decrease of poleward heat transport. Mid-latitude storms are responsible for the majority of the heat transport from the equator to the Arctic (Peixoto and Oort, 1992; Zhang and Rossow et al., 1997). In our simulations, the weakening of the Northern Hemisphere winds are shown to be robust (Fig. 4), in particular the Westerlies, which results in a reduced meridional atmospheric heat transport from the low latitudes to the Arctic (Fig. 4), leading to widespread cooling north of 60° N.

In the OGGIS simulation we see the same long range land–atmosphere–ocean teleconnection present. However, the localised effects of the increase in albedo between 9 and 6 ka, due to the diminishing LIS and the localised effects of insolation changes, results in a warming over North America. This warming emanates eastwards over the North Atlantic and the rest of northern Europe and Eurasia, as well as penetrating the Arctic, accounting for the observed warming between 9 and 6 ka in the OGGIS experiment.

Biome reconstructions of pollen and plant macrofossils show that during the mid-Holocene the Sahara was covered by grass and shrubs (Jolly et al., 1998). Claussen et al. (1999) simulated a decrease in Sahara vegetation fraction over the Holocene from 90 to 10 %. However, in our OG simulation, vegetation fraction decreases from 65 to 20 % over the same period. Therefore, we state that whilst LOVECLIM is able to capture the general pattern of vegetation changes in the Sahara it cannot capture the full amplitude of these changes. Therefore, this suggests that the impact of Sahara vegetation on Arctic cooling could be greater than the 17 % estimated. To account for this and to constrain our results we simulated extreme, early (9 ka) and late (0 ka), Holocene environments. These results enable us to place an upper limit of the potential impact of Sahara desertification has upon Arctic cooling over the Holocene. The

CPD
10, 1653–1673, 2014

results show that from a 9 ka, 100 % "green" Sahara to a 0 ka, 100 % "desert" Sahara, temperatures decrease by 4.0 °C (Fig. 2d), of which 1.7 °C (42 %) is attributable to the change in vegetation.

However, a particular weakness of LOVECLIM and our simulations that needs to be addressed is the fact that within LOVECLIM clouds are prescribed according to a modern climatology. Thus cloud cover over the Sahara in all our experiments with a standard setup is representative of cloud cover over a desert environment, hence lower latent heat flux, higher sensible heat flux and low atmospheric convection and thus reduced cloud cover. Therefore, for our experiments that contain a vegetated Sahara at 6 and 9 ka, the prescribed cloud cover is unrealistic and is likely to result in too high temperatures. With the inclusion of clouds, the incoming solar radiation reaching the surface of the Sahara at 6 and 9 ka would be reduced. However, due to the changing albedo the amount of solar radiation absorbed at the surface is likely to vary. If we perform a simple calculation of the total solar radiation absorbed at the surface in the two environments, we can easily see the difference in solar radiation absorbed at the two surfaces is quite similar. For instance, if we assume that desert albedo is 0.4, and we have a 100 % cloudless, desert environment then the downward solar radiation reaching the surface of the Sahara is 342 m^{-2} (Kiehl and Trenberth, 1997). Thus, the total solar radiation absorbed at the surface is 205 $W m^{-2}$ $[(1-0.4)\cdot 342]$. In a cloud covered, vegetated region, with surface albedo of 0.2, and assuming that 23 % of incoming solar radiation is reflected by clouds (Kiehl and Trenberth, 1997) then the downward solar radiation reaching the surface of the Sahara is 265 $W m^{-2}$ $[342\cdot(1-0.23)]$. Therefore, the solar radiation absorbed at the surface is 211 $W m^{-2}$ $[(1-0.2)\cdot(342\cdot 0.77)]$. Hence, in theory the surface of a cloudy vegetated region and that of a cloudless desert environment absorb approximately similar amounts of incoming solar radiation.

To explore this situation further we have performed a series of sensitivity experiments that included the addition of cloud cover that is representative of a vegetated region, over the Sahara. To achieve this we have taken the modern cloud cover that is

CPD
10, 1653–1673, 2014

prescribed in our model for the Amazon region and have applied it to the Sahara. Given that the Amazon region consists of trees, as opposed to a vegetated Sahara that more than likely consisted of grasses and shrubs during its vegetated period in the mid and late Holocene, this cloud cover is probably an over estimation, but still serves the purpose of assessing the impact of cloud cover over a vegetated Sahara on surface temperature. Unfortunately, due to the near total lack of proxy temperature reconstructions for the Sahara region during the early and mid-Holocene, it is not possible to verify our temperature results, but hopefully they will encourage further proxy based research into this area.

The first sensitivity experiment we performed allowed us to compare the temperature change from 6 to 0 ka for when the cloud conditions at 6 ka are both prescribed on the modern dataset and the other when we artificially induced a 6 ka cloud cover. As can be seen (Fig. 5a) the temperature difference between 6 and 0 ka with modern day cloud dataset ranges from 3 to 5 °C. With the addition of prescribed clouds at 6 ka (Fig. 5b) the temperature difference between 6 and 0 ka reduces slightly to 2–4 °C. Importantly, in both experiments the basic premise that the Sahara during the mid-Holocene was warmer than the late Holocene remains. In addition, the only temperature change observed in the Arctic occurs in the Canadian Basin and the East Siberian Sea, with a reduction in temperature by 1 °C (Fig. 5b), hence with additional clouds in the Sahara we see a slight cooling in the Arctic, which is due to the reduction of heat that is available for transportation from the low to high latitudes.

To further test the effect that prescribed clouds have upon our initial simulations we performed an additional sensitivity experiment. This experiment tested the effect of prescribed clouds during the early Holocene (9 ka). As can be seen (Table 1) when we compare the temperature changes in the Arctic at 9 ka between simulations 9k9kEQ_OG and 9k9kEQ_OG_clouds, we see that the mean annual Arctic temperatures are -11.0 ± 0.8 ° and -11.1 ± 0.8 °C respectively. This result is similar to the 6 ka sensitivity experiments, where the simulation with prescribed clouds results in a cooler Arctic. Therefore, we can say that the additional sensitivity

CPD
10, 1653–1673, 2014

experiments we performed allow us to have greater confidence with our initial findings and interpretations.

4 Concluding remarks

In conclusion we can say that over the course of the Holocene, the observed cooling in the Arctic region is not only driven by localised insolation changes, but that the effects of desertification in the Sahara initiate a long range land–atmosphere teleconnection. This teleconnection accounts for between 17 and 42 % of the observed Arctic cooling between 9 and 0 ka, with it likely that the actual effect is nearer the upper end of this range. We also show through a series of sensitivity experiments that despite an apparent weakness of our model, with its prescribed modern day cloud data set, that our overall findings are conclusive and robust, withstanding the sensitivity experiments we performed. Therefore, it can be stated that high-latitude interglacial climate is sensitive to Sahara desertification.

Appendix A

Equations to calculate the relative contributions of ORBG + GHG and Vegetation to the cooling in the Arctic, for OGGIS, OG and 100 % (extreme) runs.

- OGGIS:
  - 9 ka to 6 ka
    9k9kEQ_OGGIS – 6k6kEQ_OGGIS = Δ °C due to ALL forcings[1]
    9k9kEQ_OGGIS – 9k6kEQ_OGGIS = Δ °C due to VEGETATION forcing
    9k9kEQ_OGGIS – 6k9kEQ_OGGIS = Δ °C due to ORB & GHG forcings

CPD
10, 1653–1673, 2014

The impact of Sahara desertification on Arctic cooling during the Holocene

F. J. Davies et al.

- 6 ka to 0 ka
  6k6kEQ_OGGIS – 0k0kEQ_OGGIS = Δ °C due to ALL forcings[1]
  6k6kEQ_OGGIS – 6k0kEQ_OGGIS = Δ °C due to VEGETATION forcing
  6k6kEQ_OGGIS – 0k6kEQ_OGGIS = Δ °C due to ORB & GHG forcings

- 9 ka to 0 ka
  9k9kEQ_OGGIS – 0k0kEQ_OGGIS = Δ °C due to ALL forcings[1]
  9k9kEQ_OGGIS – 9k0kEQ_OGGIS = Δ °C due to VEGETATION forcing
  9k9kEQ_OGGIS – 0k9kEQ_OGGIS = Δ °C due to ORB & GHG forcings

[1] All forcings = GHG, ORB, prescribed Sahara vegetation, LIS and GIS topography.

- OG:

  - 9 ka to 6 ka
    9k9kEQ_OG – 6k6kEQ_OG = Δ °C due to ALL forcings[2]
    9k9kEQ_OG – 9k6kEQ_OG = Δ °C due to VEGETATION forcing
    9k9kEQ_OG – 6k9kEQ_OG = Δ °C due to ORB & GHG forcings

  - 6 ka to 0 ka
    6k6kEQ_OG – 0k0kEQ_OG = Δ °C due to ALL forcings[2]
    6k6kEQ_OG – 6k0kEQ_OG = Δ °C due to VEGETATION forcing
    6k6kEQ_OG – 0k6kEQ_OG = Δ °C due to ORB & GHG forcings

  - 9 ka to 0 ka
    9k9kEQ_OG – 0k0kEQ_OG = Δ °C due to ALL forcings[2]
    9k9kEQ_OG – 9k0kEQ_OG = Δ °C due to VEGETATION forcing
    9k9kEQ_OG – 0k9kEQ_OG = Δ °C due to ORB & GHG forcings

CPD
10, 1653–1673, 2014

– 100 %:

  – 6 ka to 0 ka
    6k100gEQ_OG – 0k100dEQ_OG = Δ °C due to ALL forcings[2]
    6k100gEQ_OG – 6k100dEQ_OG = Δ °C due to VEGETATION forcing
    6k100gEQ_OG – 0k100gEQ_OG = Δ °C due to ORB & GHG forcings

[2] All forcings = GHG, ORB and prescribed Sahara vegetation.

Acknowledgements. FJD, HR and MB are funded by the "European Communities 7th Framework Programme FP7/2013, Marie Curie Actions, under grant agreement No. 23811: CASEITN". FM is funded by the Bolin Centre for Climate Research. All support is greatly appreciated.

References

Berger, A, L.: Long-term variations of daily insolation and Quaternary climatic changes, J. Atmos. Sci., 35, 2362–2367, 1978.

Bjerknes, J.: Atlantic air–sea interaction, Adv. Geophys., 10, 1–82, 1964.

Blaschek, M. and Renssen, H.: The Holocene thermal maximum in the Nordic Seas: the impact of Greenland Ice Sheet melt and other forcings in a coupled atmosphere–sea-ice–ocean model, Clim. Past, 9, 1629–1643, doi:10.5194/cp-9-1629-2013, 2013.

Brovkin, V., Bendtsen, J., Claussen, M., Ganopolski, A., Kubatzki, C., Petoukhov, V., and Andreev., A.: Carbon cycle, vegetation and climate dynamics in the Holocene: experiments with the CLIMBER-2 model, Global Biogeochem. Cy., 16, 1139, doi:10.1029/2001GB001662, 2002

Claussen, M., Kubatzki, C., Brovkin, V., Ganopolski, A., Hoelzmann, P., and Pachur, H.-J.: Simulation of an abrupt change in Saharan vegetation in the mid-Holocene, Geophys. Res. Lett., 26, 2037–2040, 1999.

deMenocal, P., Ortiz, J., Guilderson, T., Adkins, J., Sarnthein, M., Baker, L., and Yarusinsky, M.: Abrupt onset and termination of the African Humid Period: rapid climate responses to gradual insolation forcing, Quaternary Sci. Rev., 19, 347–361, 2000

CPD
10, 1653–1673, 2014

Deleersnijder, E. and Campin, J.-M.: On the computation of the barotropic mode of a free-surface world ocean model, Ann. Geophys., 13, 675–688, doi:10.1007/s00585-995-0675-x, 1995.
Deleersnijder, E., Beckers, J. M., Campin, J. M., El Mohajir, M., Fichefet, T., and Luyten, P.: Some mathematical problems associated with the development and use of marine models, in: The Mathematics of Model for Climatology and Environment, edited by: Diaz, J. I., NATO ASI Series, Springer Berlin Heidelberg, 48, 39–86, 1997.
Fichefet, T. and Morales Maqueda, M. A.: Sensitivity of a global sea ice model to the treatment of ice thermodynamics and dynamics, J. Geophys. Res., 102, 12609–12646, 1997.
Fichefet, T. and Morales Maqueda, M. A.: Modelling the influence of snow accumulation and snow-ice formation on the seasonal cycle of the Antarctic sea-ice cover, Clim. Dynam.15, 251–268, 1999.
Goosse, H., Brovkin, V., Fichefet, T., Haarsma, R., Huybrechts, P., Jongma, J., Mouchet, A., Selten, F., Barriat, P.-Y., Campin, J.-M., Deleersnijder, E., Driesschaert, E., Goelzer, H., Janssens, I., Loutre, M.-F., Morales Maqueda, M. A., Opsteegh, T., Mathieu, P.-P., Munhoven, G., Pettersson, E. J., Renssen, H., Roche, D. M., Schaeffer, M., Tartinville, B., Timmermann, A., and Weber, S. L.: Description of the Earth system model of intermediate complexity LOVECLIM version 1.2, Geosci. Model Dev., 3, 603–633, doi:10.5194/gmd-3-603-2010, 2010.
Haarsma, R. J., Selten, F. M., Opsteegh, J. D., Lenderink, G., and Liu, Q.: A coupled atmosphere ocean sea-ice model for climate predictability studies, KNMI, De Bilt, the Netherlands, 31 pp., 1996.
Jolly, D., Prentice, I.C, Bonnefille, R., Ballouche, A., Bengo, M., Brenac, P., Buchet, G., Burney, D., Cazet, J. P., Cheddadi, R., Edorh, T., Elenga, H., Elmoutaki, S., Guiot, J., Laarif, F., Lamb, H., Lezine, A. M., Maley, J., Mbenza, M., Peyron, O., Reille, M., Reynaud-Farrera, I., Riollet, G., Ritchie, J. C., Roche, E., Scott, L., Ssemmanda, I., Straka, H., Umer, M., Van Campo, E., Vilimumbalo, S., Vincens, A., and Waller, M.: Biome reconstruction from pollen and plant macrofossil data for Africa and the Arabian peninsula at 0 and 6000 years, J. Biogeogr., 25, 1007–1027, 1998.
Kiehl, J. T. and Trenberth, K. E.: Earth's annual global mean energy budget, B. Am. Meteorol. Soc., 78, 197–208, 1997.
Kröpelin, S., Verschuren, D., Lézine, A. M., Eggermont, H., Cocquyt, C., Francus, P., Cazet, J.-P., Fagot, M., Rumes, B., Russell, J. M., Darius, F., Conley, D. J., Schuster, M., von

CPD
10, 1653–1673, 2014

The impact of Sahara desertification on Arctic cooling during the Holocene

F. J. Davies et al.

Suchodoletz, H., and Engstrom., D. R.: Climate-driven ecosystem succession in the Sahara: the past 6000 years, Science, 320, 765–768, 2008.
Kutzbach, J. E. and Street-Perrott, F. A.: Milankovitch forcing of fluctuations in the level of tropical lakes from 18 to 0 kyr BP, Nature, 317, 130–134, 1985.
Licciardi, J. M., Teller, J. T., and Clark, P. U.: Freshwater routing by the Laurentide Ice Sheet during the last deglaciation, in: Mechanisms of Global Climate Change at Millennial Time Scales, edited by: Clark, P. U., Webb, R. S., and Keigwin, L. D., American Geophysical Union, Washington, DC, Geophysical Monograph, 112, 177–201, 1999.
Loulergue, L., Schilt, A., Spahni, R., Masson-Delmotte, V., Blunier, T., Lemieux, B., Barnola, J. M., Raynaud, D., Stockern, T. F., and Chappellaz, J.: Orbital and millennial-scale features of atmospheric CH_4 over the past 800,000 years, Nature, 453, 383–386, 2008.
Opsteegh, J. D., Haarsma, R. J., Selten, F. M., and Kattenberg, A.: ECBilt: a dynamic alternative to mixed boundary conditions in ocean models, Tellus A, 50, 348–367, 1998.
Peixoto, J. P. and Oort, A. H.: Physics of Climate, American Institute of Physics, New York, 520 pp., 1992.
Peltier, W.: Global glacial isostasy and the surface of the Ice-Age Earth: the ICE-5G (VM2) model and grace, Annu. Rev. Earth Pl. Sc., 32, 111–149, doi:10.1146/annurev.earth.32.082503.144359, 2004.
Renssen, H., Goosse, H., Fichefet, T., Brovkin, V., Driesschaert, E., and Wolk, F.: Simulating the Holocene climate evolution at northern high latitudes using a coupled atmosphere–sea ice–ocean–vegetation model, Clim. Dynam., 24, 23–43, 2005.
Renssen, H., Driesschaert, E., Loutre, M. F., and Fichefet, T.: On the importance of initial conditions for simulations of the Mid-Holocene climate, Clim. Past, 2, 91–97, doi:10.5194/cp-2-91-2006, 2006.
Renssen, H., Seppä, H., Heiri, O., Roche, D. M., Goosse, H., and Fichefet, T.: The spatial and temporal complexity of the Holocene thermal maximum, Nat. Geosci., 2, 411–414, doi:10.1038/NGEO513, 2009.
Schilt, A., Baumgartner, M., Blunier, T., Schwander, J., Spahni, R., Fischer, H., and Stocker, T. F.: Glacial–interglacial and millennial-scale variations in the atmospheric nitrous oxide concentration during the last 800,000 years, Quaternary Sci. Rev., 29, 182–192, 2010.
Zhang, Y.-C. and Rossow, W. B.: Estimating meridional energy transports by the atmospheric and oceanic general circulations using boundary fluxes, J. Climate, 10, 2358–2373, 1997.

CPD
10, 1653–1673, 2014

Table 1. Equilibrium experiments that were performed and the mean annual Arctic (66.5° N) temperature for each simulation.

OGGIS				Arctic temp. (°C)	
ORB + GHG	VEG	TYPE	NAME	temp	s.d. (±)
0 ka	0 ka	EQ	0k0kEQ_OGGIS	−13.9	0.9
0 ka	6 ka	EQ	0k6kEQ_OGGIS	−13.5	0.9
0 ka	9 ka	EQ	0k9kEQ_OGGIS	−13.2	1.0
6 ka	0 ka	EQ	6k0kEQ_OGGIS	−12.2	0.8
6 ka	6 ka	EQ	6k6kEQ_OGGIS	−11.8	0.8
6 ka	9 ka	EQ	6k9kEQ_OGGIS	−11.5	0.8
9 ka	0 ka	EQ	9k0kEQ_OGGIS	−13.5	0.9
9 ka	6 ka	EQ	9k6kEQ_OGGIS	−13.0	0.9
9 ka	9 ka	EQ	9k9kEQ_OGGIS	−12.8	0.9
OG				**Arctic temp. (°C)**	
ORB + GHG	VEG	TYPE	NAME	temp	s.d. (±)
0 ka	0 ka	EQ	0k0kEQ_OG	−13.9	1.0
0 ka	6 ka	EQ	0k6kEQ_OG	−13.5	1.0
0 ka	9 ka	EQ	0k9kEQ_OG	−13.1	1.0
6 ka	0 ka	EQ	6k0kEQ_OG	−12.2	0.8
6 ka	6 ka	EQ	6k6kEQ_OG	−11.8	0.8
6 ka	9 ka	EQ	6k9kEQ_OG	−11.5	0.8
9 ka	0 ka	EQ	9k0kEQ_OG	−11.6	0.8
9 ka	6 ka	EQ	9k6kEQ_OG	−11.2	0.8
9 ka	9 ka	EQ	9k9kEQ_OG	−11.0	0.8
9 ka	9 ka	EQ	9k9kEQ_OG_clouds	−11.1	0.8

Discussion Paper | Discussion Paper | Discussion Paper | Discussion Paper |

CPD
10, 1653–1673, 2014

Table 2. Extreme experiments that were performed and the mean annual Arctic (66.5° N) temperature for each simulation.

Simulation				Arctic temp. (°C)	
ORB + GHG	VEG	TYPE	NAME	temp	s.d. (±)
9 ka	100 % Grass	EQ	9k100gEQ	−10.5	0.8
9 ka	100 % Desert	EQ	9k100dEQ	−12.1	0.8
6 ka	100 % Grass	EQ	6k100gEQ_clouds	−11.3	0.8
6 ka	100 % Grass	EQ	6k100gEQ	−10.9	0.8
6 ka	100 % Desert	EQ	6k100dEQ	−12.7	0.8
0 ka	100 % Grass	EQ	0k100gEQ	−12.5	0.9
0 ka	100 % Desert	EQ	0k100dEQ	−14.5	0.9

CPD
10, 1653–1673, 2014

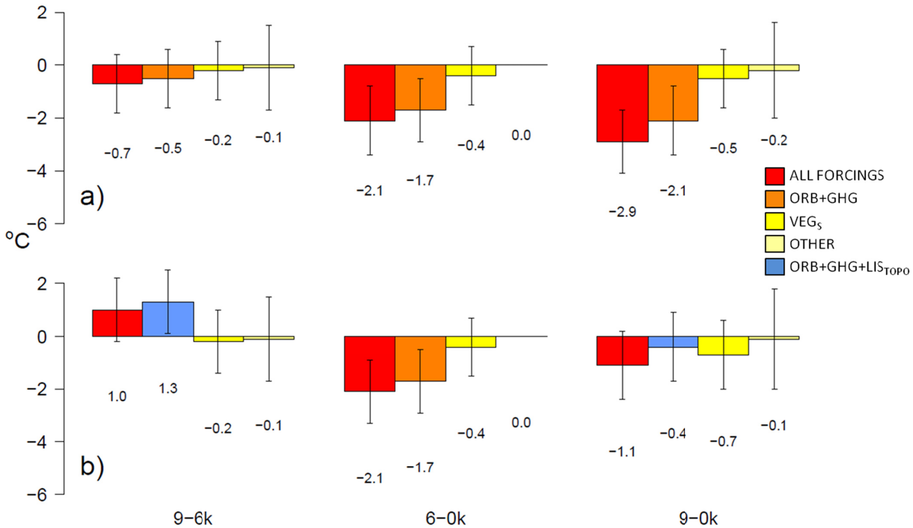

Fig. 1. Simulated temperature change in the Arctic for **(a)** OG and **(b)** OGGIS equilibrium simulations, showing the relative contributions of different forcings; ORB + GHG (Orbital and Greenhouse gases), VEG$_S$ (Vegetation changes in the Sahara), OTHER (other factors outside the Sahara region such as vegetation changes), ORB + GHG + LISTOPO (Orbital and Greenhouse Gases and Laurentide Icesheet Topography, which is only relevant for the period 9–6 ka) and ALL (For OG this includes: GHG, ORB and prescribed Sahara vegetation; for OGGIS this includes: GHG, ORB, prescribed Sahara vegetation, LIS melt, GIS melt and LIS topography changes). Error bars represent $\pm 1\sigma$.

CPD
10, 1653–1673, 2014

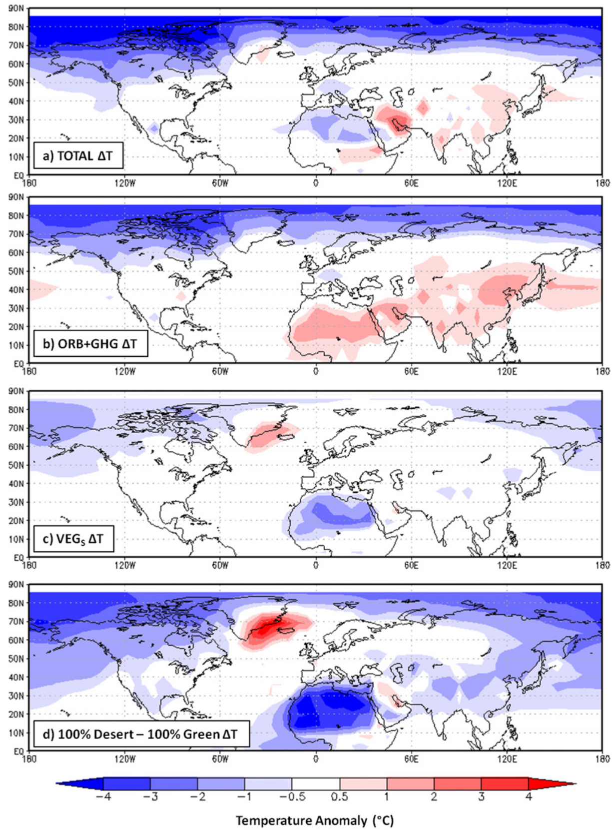

Fig. 2. Surface temperature anomaly plots from the OG equilibrium simulation from 9 to 0 ka showing the relative contributions of **(a)** ALL (0–9 ka); **(b)** ORB + GHG (0–9 ka); **(c)** VEG (0–9 ka); and **(d)** 100 % Desert Sahara – 100 % Green Sahara (0 ka) forcings upon global climate. Values are 500 year means.

CPD
10, 1653–1673, 2014

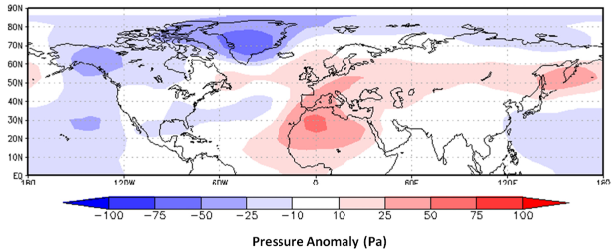

Fig. 3. 9k0kEQ–9k9kEQ_OG 800 hPa Geopotential Height, allowing the effects of changing vegetation in the Sahara, on pressure, to be visualised.

CPD
10, 1653–1673, 2014

Title Page
Abstract | Introduction
Conclusions | References
Tables | Figures
Back | Close
Full Screen / Esc
Printer-friendly Version
Interactive Discussion

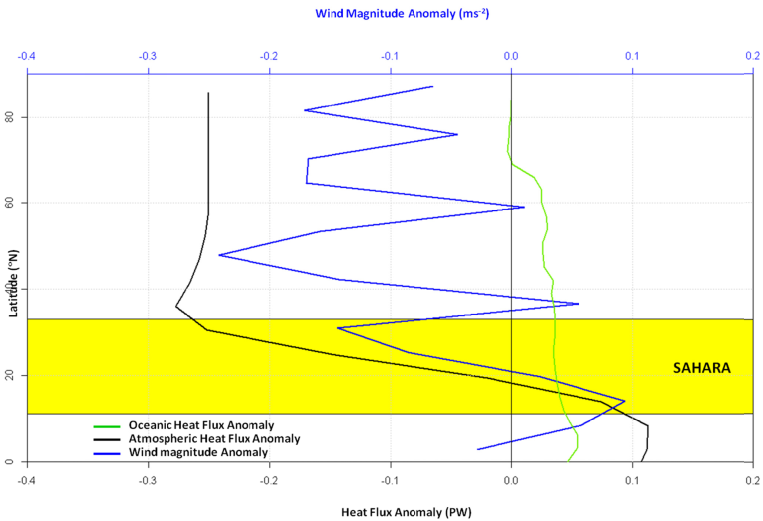

Fig. 4. Depicts both the (i) mean annual oceanic heat flux anomaly (PW), (ii) mean annual atmospheric heat flux anomaly (PW), and (iii) mean annual wind magnitude anomaly (ms^{-2}) over the North Atlantic (defined as 60° W–15° E) (9k0kEQ_OG–9k9kEQ_OG). The latitudinal extent of the Sahara is highlighted for reference.

CPD
10, 1653–1673, 2014

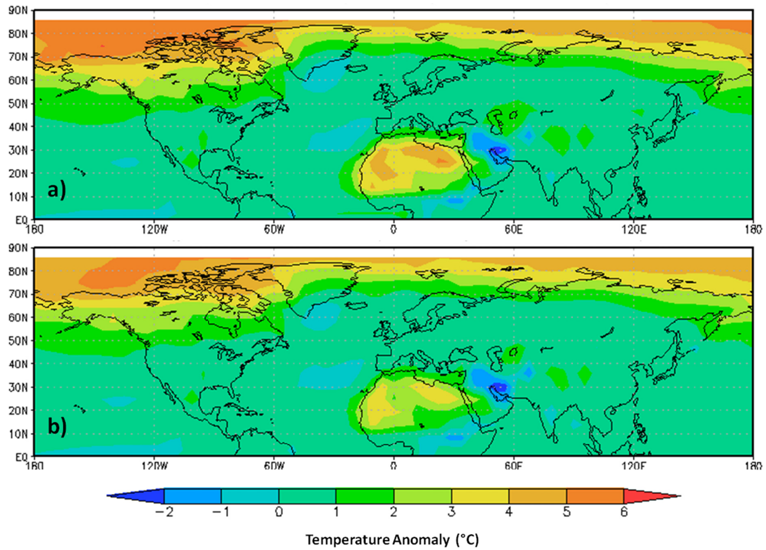

Fig. 5. Temperature change between **(a)** 6k Green Sahara–0k Sahara with modern day clouds prescribed (6k100gEQ–0k100dEQ) and **(b)** 6k Green Sahara with 6k prescribed clouds–0k Sahara (6k100gEQ_clouds–0k100dEQ).

CPD
10, 1653–1673, 2014

The impact of Sahara desertification on Arctic cooling during the Holocene

F. J. Davies et al.